Nodal collocation method for the multidimensional P_L equations applied to neutron transport source problems

M. T. Capilla[a], C. F. Talavera[a], D. Ginestar[a], G. Verdú[b,*]

[a] *Departamento de Matemática Aplicada. Universitat Politècnica de València. Camino de Vera 14. E-46022 Valencia, Spain.*

[b] *Departamento de Ingeniería Química y Nuclear. Universitat Politècnica de València. Camino de Vera 14, E-46022 Valencia, Spain.*

Abstract

A P_L spherical harmonics-nodal collocation method is applied to the solution of the multidimensional neutron source transport equation. Vacuum boundary conditions are approximated by setting Marshak's conditions. The method is applied to several 1D, 2D and 3D problems with isotropic fixed source and with isotropic and anisotropic scattering. These problems are chosen to test this method in limit conditions, showing that in some cases a high order P_L approximation is required to obtain accurate results and convergence. Results are also compared with the ones provided by several reference codes showing good agreement. It is also shown that Marshak's approximation to vacuum boundary conditions gives the same results that simulating vacuum with a purely absorbing medium and setting zero flux boundary conditions.

Keywords: Multidimensional P_L equations; Spherical harmonics; Nodal collocation method; Three-dimensional neutron source benchmarks; Marshak's vacuum boundary conditions.

1. Introduction

Neutron transport theory is of great interest in many applications such as nuclear reactors, nuclear medicine, radiological protection, etc. The phys-

*Corresponding author. Tel.: 34-963877630; fax: 34-963877639.

Email addresses: tcapilla@mat.upv.es (M. T. Capilla), talavera@mat.upv.es (C. F. Talavera), dginesta@mat.upv.es (D. Ginestar), gverdu@iqn.upv.es (G. Verdú)

ical phenomena of neutron transport are described by the neutron transport equation, which is a balance equation in a space of seven dimensions. Except for academical problems, the solution of this equation is obtained using Monte Carlo methods (Spanier and Gelbard, 2008) or other numerical methods (Lewis and Miller, 1984). Both kind of methods are very expensive from the computational point of view. To solve this problem, several approximations have been introduced to simplify the neutron transport equation. One of the most popular is the discrete ordinates method (S_N equations) implemented in several codes such as DANTSYS (Alcouffe et al., 1995), PENTRAN (Sjoden and Haghighat, 1996), DORT/TORT (Rhoades and Childs, 1993) and DRAGON (Marleau et al., 2008). This method is based on considering a finite set of angular directions and their corresponding weights that define an appropriate quadrature set in the unit sphere (Sánchez and McCormick, 1982). The main drawback of this kind of methods is that they suffer of ray effects, that is, they provide non-physical solutions for certain configurations. Another possibility is to use the P_L equations (Weinberger and Wigner, 1958; Gelbard, 1968), which are obtained expanding the angular dependence of the angular neutron flux and the nuclear cross-sections in terms of a finite number of spherical harmonics. An advantage of the spherical harmonics method is that the equations are invariant under rotation of the co-ordinates and do not depend on the direction of the co-ordinates that should give no ray effects. The P_L equations are complicated and need a particular treatment. Simplified P_L approximations have been proposed (Gelbard, 1968), which can be easily implemented using essentially the same numerical methods as the ones used for the diffusion equation.

Also, numerical modeling of photon transport through tissue has become well established in tomography and has often been described by the diffusion approximation to the transport equation (Aydin et al., 2005). The diffusion approximation is, however, valid only for regions that are much more scattering than absorbing. Thus, in problems of non-scattering regions the diffusion approximation fails and higher order approximations to transport equations are needed.

Two kind of calculations are typically performed using the neutron transport equations: criticality calculations, where the k-effective and the neutron distribution for a stationary configuration of a multiplying system are determined, and fixed source calculations, where a neutron source is placed in a medium determining the resulting neutron distribution. In previous works (Capilla et al., 2005, 2008, 2012), a nodal collocation method was developed for the P_L equations; the method was implemented into a computer code called SHNC (Spherical Harmonics Nodal Collocation) and then applied to criticality calculations. In this work, this method has been extended to study different neutron source problems in multidimensional geometries, comparing the obtained results with reference results provided in the literature. We want to remark that all the methods developed in this paper can be also applied to the photon transport equation.

The rest of the paper is organized as follows. Section 2 is devoted to a review of the derivation of the P_L equations in multidimensional geometries. In Section 3, a brief review of the nodal collocation method used for the spatial discretization is presented. In Section 4, the performance of the nodal collocation method for the P_L equations is analyzed using different neutron source problems in 1D, 2D and 3D geometries. Finally, the main conclusions of the study are summarized in Section 5.

2. The transport equation and the P_L equations

In this section we review the multi-dimensional P_L equations, for arbitrary angular order L, that will be formulated as vector-valued second order differential equations. Boundary conditions will also be computed for arbitrary order L. Vacuum boundary conditions are approximated using Marshak's conditions. Reflective boundary conditions, on the contrary, can be treated in an exact way. The approximation of zero flux boundary conditions will also be considered.

The first-order neutron transport equation (Stacey, 2001) is

$$\begin{aligned}\vec{\Omega}\,\vec{\nabla}\Phi(\vec{r},\vec{\Omega},E) + \Sigma_t(\vec{r},E)\,\Phi(\vec{r},\vec{\Omega},E) \\ = Q_s(\vec{r},\vec{\Omega},E) + Q_f(\vec{r},\vec{\Omega},E) + S(\vec{r},\vec{\Omega},E)\,, \quad (1)\end{aligned}$$

where $\Phi(\vec{r},\vec{\Omega},E)$ is the neutron angular flux at location $\vec{r}=(x_1,x_2,x_3)$ (in Cartesian coordinates) with energy E and direction given by the unit vector $\vec{\Omega}=(\cos\varphi\,\sin\theta\,,\,\sin\varphi\,\sin\theta\,,\,\cos\theta)$, $0<\varphi<2\pi$, $0<\theta<\pi$; Σ_t is the total macroscopic cross-section; S is the fixed source term and Q_s and Q_f are the scattering source term and the source of neutrons by fission term respectively, given by:

$$
\begin{aligned}
Q_s(\vec{r},\vec{\Omega},E) &= \int dE' \int d\vec{\Omega}'\, \Sigma_s(\vec{r};\vec{\Omega}',E' \to \vec{\Omega},E)\, \Phi(\vec{r},\vec{\Omega}',E')\,, \\
Q_f(\vec{r},\vec{\Omega},E) &= \frac{\chi_p(E)}{4\pi} \int dE'\, \nu\Sigma_f(\vec{r},E') \int d\vec{\Omega}'\, \Phi(\vec{r},\vec{\Omega}',E')\,,
\end{aligned}
$$

where Σ_s is the scattering cross-section from $(\vec{\Omega}',E')$ to $(\vec{\Omega},E)$; Σ_f is the fission cross-section; ν is the average number of neutrons per fission and χ_p is the spectrum.

In practical applications, to eliminate the dependence of energy in Eq. (1), an energy multi-group approximation is used. In order to facilitate the notation we will consider the monoenergetic version of these equations. For the extension of the nodal collocation method to G energy groups, $\Phi(\vec{r},\vec{\Omega})$ is replaced by a column vector of G components corresponding to each energy group, Σ_t is a diagonal matrix and Σ_s, $\nu\Sigma_f$ are also adequate matrices.

In the spherical harmonics method the angular dependence of the neutronic flux $\Phi(\vec{r},\vec{\Omega})$ and the source term $S(\vec{r},\vec{\Omega})$ are expanded in terms of the (complex) spherical harmonics $Y_l^m(\vec{\Omega}) = \sqrt{\frac{(2l+1)}{4\pi}\frac{(l-m)!}{(l+m)!}}\, P_l^m(\cos\theta)e^{im\varphi}$ (Courant et al., 1962) (where $P_l^m(\cos\theta)$ are the associated Legendre polynomials), that form a complete set of orthonormal functions, that is, they satisfy the orthonormality property $\int d\vec{\Omega}\, {Y_m^l}^* Y_{m'}^{l'} = \delta_{ll'}\delta_{mm'}$, where δ_{ij} is the Kronecker delta and $d\vec{\Omega} = \sin\theta\, d\varphi d\theta$, $0 < \varphi < 2\pi$, $0 < \theta < \pi$. Thus,

$$
\Phi(\vec{r},\vec{\Omega}) = \sum_{l=0}^{\infty} \sum_{m=-l}^{+l} \phi_{lm}(\vec{r})\, Y_l^m(\vec{\Omega})\,, \qquad S(\vec{r},\vec{\Omega}) = \sum_{l=0}^{\infty} \sum_{m=-l}^{+l} s_{lm}(\vec{r})\, Y_l^m(\vec{\Omega})\,, \tag{2}
$$

where $\phi_{lm}(\vec{r})$ and $s_{lm}(\vec{r})$ are the (spherical harmonics) moments. Complex spherical harmonics will provide a more concise theoretical description of the method. We observe that the transport equation (1) is a real equation and, as we are interested (for physical reasons) on real solutions, then $\Phi = \Phi^*$, that is, ${\phi_{lm}}^* = (-1)^m \phi_{l,-m}$ and not all complex moments are independent so there are only $2l+1$ real independent moments for each $l > 0$, that is, $\{\phi_{l0}, \mathrm{Re}\,\phi_{lm}, \mathrm{Im}\,\phi_{lm}, m = 1,\ldots,l\}$. The real form of the equations is more convenient from the computational point of view.

It will also be assumed that scattering depends only on the relative angle between the incident and the scattered neutrons, $\vec{\Omega}\,\vec{\Omega}'$, and that the scattering cross-section may be expanded as the following series of Legendre polynomials

$$\Sigma_s(\vec{r},\vec{\Omega}\,\vec{\Omega}') = \sum_{l=0}^{\infty} \frac{2l+1}{4\pi} \Sigma_{s,l}(\vec{r})\, P_l(\vec{\Omega}\,\vec{\Omega}') \ . \tag{3}$$

Expansions (2) and (3) and the orthogonality properties of Y_l^m are then used into Eq. (1). Let us consider the first term in Eq. (1) (that accounts for neutrons removed by leakage in direction $\vec{\Omega}$). If $\vec{\Omega}\,\vec{\nabla}\Phi(\vec{r},\vec{\Omega}) = \sum_{l'=0}^{\infty}\sum_{m'=-l'}^{+l'} A_{l'm'}(\vec{r})Y_{l'}^{m'}(\vec{\Omega})$ then (we omit arguments for clarity)

$$\begin{aligned} A_{l'm'} &= \int d\vec{\Omega}\, Y_{l'}^{m'*}(\vec{\Omega}\,\vec{\nabla}\Phi) \\ &= \sum_{\substack{l=0 \\ -l\le m\le +l}}^{\infty} \Big[\int d\vec{\Omega}\, Y_{l'}^{m'*}\cos\varphi\sin\theta\, Y_l^m\, \frac{\partial\phi_{lm}}{\partial x_1} + \int d\vec{\Omega}\, Y_{l'}^{m'*}\sin\varphi\sin\theta\, Y_l^m\, \frac{\partial\phi_{lm}}{\partial x_2} \\ &\qquad + \int d\vec{\Omega}\, Y_{l'}^{m'*}\cos\theta\, Y_l^m\, \frac{\partial\phi_{lm}}{\partial x_3}\Big] . \end{aligned} \tag{4}$$

If we have into account the following formulas

$$\begin{aligned} &\int d\vec{\Omega}\, Y_{l'}^{m'*}\sin\theta\, e^{-i\varphi}\, Y_l^m = \big(-C_1(l,m)\delta_{l-1,l'} + C_2(l',m')\delta_{l'-1,l}\big)\delta_{m'+1,m} \ , \\ &\int d\vec{\Omega}\, Y_{l'}^{m'*}\sin\theta\, e^{i\varphi}\, Y_l^m = \big(-C_1(l',m')\delta_{l'-1,l} + C_2(l,m)\delta_{l-1,l'}\big)\delta_{m+1,m'} \ , \\ &\int d\vec{\Omega}\, Y_{l'}^{m'*}\cos\theta\, Y_l^m = \big(C_3(l,m)\delta_{l-1,l'} + C_3(l',m')\delta_{l'-1,l}\big)\delta_{m',m} \ , \end{aligned}$$

where

$$\begin{aligned} C_1(l,m) &= \left(\frac{(l+m)(l+m-1)}{(2l+1)(2l-1)}\right)^{1/2} \ , \quad C_2(l,m) = C_1(l,-m)\,, \\ C_3(l,m) &= \left(\frac{(l+m)(l-m)}{(2l+1)(2l-1)}\right)^{1/2} \ , \end{aligned}$$

it follows that

$$A_{l'm'} = \sum_{\substack{l=0 \\ -l\le m\le +l}}^{\infty} \Bigg\{\frac{1}{2}\Big[\big(-C_1(l,m)\delta_{l-1,l'} + C_2(l',m')\delta_{l'-1,l}\big)\delta_{m'+1,m}$$

$$
\begin{aligned}
&\quad + \big(-C_1(l',m')\delta_{l'-1,l} + C_2(l,m)\delta_{l-1,l'}\big)\delta_{m+1,m'}\Big]\frac{\partial\phi_{lm}}{\partial x_1} \\
&+ \frac{1}{2i}\Big[\big(-C_1(l,m)\delta_{l-1,l'} + C_2(l',m')\delta_{l'-1,l}\big)\delta_{m'+1,m} \\
&\quad + \big(-C_1(l',m')\delta_{l'-1,l} + C_2(l,m)\delta_{l-1,l'}\big)\delta_{m+1,m'}\Big]\frac{\partial\phi_{lm}}{\partial x_2} \\
&+ \big(C_3(l,m)\delta_{l-1,l'} + C_3(l',m')\delta_{l'-1,l}\big)\delta_{m',m}\frac{\partial\phi_{lm}}{\partial x_3}\Bigg\}\,.
\end{aligned}
\tag{5}
$$

Let us now consider the scattering source term in Eq. (1). Knowing that the Legendre polynomials of a scalar product of unit vectors can be expanded as $P_l(\vec{\Omega}\,\vec{\Omega}') = \frac{4\pi}{2l+1}\sum_{m=-l}^{l} Y_l^m(\vec{\Omega})Y_l^{m*}(\vec{\Omega}')$, and using the assumption (3), we get

$$
\begin{aligned}
Q_s(\vec{r},\vec{\Omega}) &= \int d\vec{\Omega}' \sum_{l=0}^{\infty} \frac{2l+1}{4\pi}\Sigma_{s,l}(\vec{r})P_l(\vec{\Omega}\,\vec{\Omega}')\Phi(\vec{r},\vec{\Omega}') \\
&= \int d\vec{\Omega}' \sum_{l=0}^{\infty}\sum_{m=-l}^{l} \Sigma_{s,l}(\vec{r})Y_l^m(\vec{\Omega})Y_l^{m*}(\vec{\Omega}')\Phi(\vec{r},\vec{\Omega}') = \sum_{\substack{l=0\\ -l\le m\le +l}}^{\infty} \Sigma_{s,l}\, Y_l^m(\vec{\Omega})\phi_{lm}(\vec{r})\,.
\end{aligned}
\tag{6}
$$

From these expressions it is straightforward to obtain the following (infinite) set of (complex) equations for the spherical harmonics moments ϕ_{lm}:

$$
\begin{aligned}
&\frac{1}{2}\Big(-C_1(l+1,m+1)\frac{\partial\phi_{l+1,m+1}}{\partial x_1} + C_2(l,m)\frac{\partial\phi_{l-1,m+1}}{\partial x_1} \\
&\qquad - C_1(l,m)\frac{\partial\phi_{l-1,m-1}}{\partial x_1} + C_2(l+1,m-1)\frac{\partial\phi_{l+1,m-1}}{\partial x_1}\Big) \\
&+ \frac{1}{2i}\Big(-C_1(l+1,m+1)\frac{\partial\phi_{l+1,m+1}}{\partial x_2} + C_2(l,m)\frac{\partial\phi_{l-1,m+1}}{\partial x_2} \\
&\qquad - C_1(l,m)\frac{\partial\phi_{l-1,m-1}}{\partial x_2} + C_2(l+1,m-1)\frac{\partial\phi_{l+1,m-1}}{\partial x_2}\Big) \\
&+ C_3(l+1,m)\frac{\partial\phi_{l+1,m}}{\partial x_3} + C_3(l,m)\frac{\partial\phi_{l-1,m}}{\partial x_3} + \Sigma_t\,\phi_{lm} \\
&\quad = \Sigma_{s,l}\,\phi_{lm} + \delta_{l0}\delta_{m0}\,\nu\Sigma_f\,\phi_{00} + s_{lm}\,, \qquad l = 0,1,\ldots\,, \quad m = -l,\ldots,+l\,,
\end{aligned}
\tag{7}
$$

It is understood that terms involving moments ϕ_{lm} with invalid indices l and m are zero. To obtain a finite approximation, the series in expansions (2) and (3) are truncated at some finite order $l = L$ and the resulting Eq. (7) are known as the P_L equations. In the following, we will only consider L to be an odd integer.

We will now obtain the real form of P_L equations (7). From previous comments, we have that for each $l = 0, 1, \ldots, L$, only equations with index $m \geq 0$ are independent; taking real and imaginary part in Eq. (7) and defining the real moments

$$\begin{aligned} \xi_{lm} &= \operatorname{Re}\phi_{lm} = \frac{1}{2}(\phi_{lm} + (-1)^m \phi_{l,-m})\,, \\ \eta_{lm} &= \operatorname{Im}\phi_{lm} = \frac{1}{2i}(\phi_{lm} - (-1)^m \phi_{l,-m})\,, \end{aligned} \tag{8}$$

we obtain the corresponding $2l+1$ real equations:

$$\begin{aligned} &\frac{1}{2}\Big(-C_1(l+1,m+1)\frac{\partial \xi_{l+1,m+1}}{\partial x_1} + C_2(l,m)\frac{\partial \xi_{l-1,m+1}}{\partial x_1} \\ &\qquad - C_1(l,m)\frac{\partial \xi_{l-1,m-1}}{\partial x_1} + C_2(l+1,m-1)\frac{\partial \xi_{l+1,m-1}}{\partial x_1}\Big) \\ &+ \frac{1}{2}\Big(-C_1(l+1,m+1)\frac{\partial \eta_{l+1,m+1}}{\partial x_2} + C_2(l,m)\frac{\partial \eta_{l-1,m+1}}{\partial x_2} \\ &\qquad - C_1(l,m)\frac{\partial \eta_{l-1,m-1}}{\partial x_2} + C_2(l+1,m-1)\frac{\partial \eta_{l+1,m-1}}{\partial x_2}\Big) \\ &+ C_3(l+1,m)\frac{\partial \xi_{l+1,m}}{\partial x_3} + C_3(l,m)\frac{\partial \xi_{l-1,m}}{\partial x_3} + \Sigma_t\,\xi_{lm} \\ &\quad = \Sigma_{s,l}\,\xi_{lm} + \delta_{l0}\delta_{m0}\,\nu\Sigma_f\,\xi_{00} + \operatorname{Re}s_{lm}\,, \qquad m = 0, 1, \ldots, l\,, \end{aligned} \tag{9a}$$

and

$$
\begin{aligned}
&\frac{1}{2}\Big(-C_1(l+1,m+1)\frac{\partial \eta_{l+1,m+1}}{\partial x_1}+C_2(l,m)\frac{\partial \eta_{l-1,m+1}}{\partial x_1}\\
&\qquad -C_1(l,m)\frac{\partial \eta_{l-1,m-1}}{\partial x_1}+C_2(l+1,m-1)\frac{\partial \eta_{l+1,m-1}}{\partial x_1}\Big)\\
&-\frac{1}{2}\Big(-C_1(l+1,m+1)\frac{\partial \xi_{l+1,m+1}}{\partial x_2}+C_2(l,m)\frac{\partial \xi_{l-1,m+1}}{\partial x_2}\\
&\qquad -C_1(l,m)\frac{\partial \xi_{l-1,m-1}}{\partial x_2}+C_2(l+1,m-1)\frac{\partial \xi_{l+1,m-1}}{\partial x_2}\Big)\\
&+C_3(l+1,m)\frac{\partial \eta_{l+1,m}}{\partial x_3}+C_3(l,m)\frac{\partial \eta_{l-1,m}}{\partial x_3}+\Sigma_t\,\eta_{lm}\\
&\quad=\Sigma_{s,l}\,\eta_{lm}+\operatorname{Im} s_{lm}\,,\qquad m=1,\ldots,l\,,
\end{aligned}
\tag{9b}
$$

From the index structure of Eqs. (9a, 9b) it is convenient to gather even l moments into vectors $X=(\xi_{l,m\geq 0},\eta_{l,m>0})_{l=\text{even}}$ and $\mathcal{S}=(\operatorname{Re} s_{l,m\geq 0},\operatorname{Im} s_{l,m>0})_{l=\text{even}}$, with $n_e=L(L+1)/2$ components, and odd l moments into vectors $\bar{X}=(\xi_{l,m\geq 0},\eta_{l,m>0})_{l=\text{odd}}$ and $\bar{\mathcal{S}}=(\operatorname{Re} s_{l,m\geq 0},\operatorname{Im} s_{l,m>0})_{l=\text{odd}}$, with $n_o=(L+1)(L+2)/2$ components (for example, if $L=1$ then $X=(\xi_{00})$ and $\bar{X}=(\xi_{10},\xi_{11},\eta_{11})^T$). Then Eqs. (9a, 9b) can be rewritten as

$$
\sum_{j=1}^{3} M_j\frac{\partial \bar{X}}{\partial x_j}+\operatorname{diag}(\Sigma_t-\Sigma_{sl})_{l=\text{even}}X=\operatorname{diag}(\delta_{l0}\,\nu\Sigma_f)_{l=\text{even}}X+\mathcal{S}\,, \tag{10}
$$

$$
\sum_{j=1}^{3} \bar{M}_j\frac{\partial X}{\partial x_j}+\operatorname{diag}(\Sigma_t-\Sigma_{sl})_{l=\text{odd}}\bar{X}=\bar{\mathcal{S}}\,, \tag{11}
$$

where M_j and $\bar{M}_j$ are rectangular matrices (of dimension $n_e\times n_o$ and $n_o\times n_e$, respectively) defined from the coefficients of Eqs. (9a,9b). Eq. (11) relates $\bar{X}$ with derivatives of X so it corresponds to a generalization of "Fick's law":

$$
\bar{X}=-D\sum_{j=1}^{3}\bar{M}_j\frac{\partial X}{\partial x_j}+D\,\bar{\mathcal{S}}\,, \tag{12}
$$

where $D=\operatorname{diag}(\Sigma_t-\Sigma_{sl})^{-1}_{l=\text{odd}}$ is a square matrix. Replacing Eq. (12) into Eq. (10) we obtain the "diffusive form of P_L equations"

$$
-\sum_{i,j=1}^{3}\frac{\partial}{\partial x_i}\Big(M_iD\bar{M}_j\frac{\partial X}{\partial x_j}\Big)+\big(\Sigma_a-\operatorname{diag}(\delta_{l0}\,\nu\Sigma_f)_{l=\text{even}}\big)X=\mathcal{S}_{\text{eff}}\,, \tag{13}
$$

where $\Sigma_a = \text{diag}(\Sigma_t - \Sigma_{sl})_{l=\text{even}}$ and the "effective source term" is $\mathcal{S}_{\text{eff}} = \mathcal{S} - \sum_{j=1}^{3} \frac{\partial}{\partial x_j}(M_j D \bar{\mathcal{S}})$. The (square) "effective diffusion matrices" $M_i D \bar{M}_j$ generalize the diffusion coefficient $1/(3(\Sigma_t - \Sigma_{s1}))$ of P_1 equation to P_L equations for $L > 1$. Notice that Eq. (13) will encounter difficulties when dealing with problems that involve void regions, where matrix D is (near) singular.

Finally, Eq. (13) corresponds to 3D geometry. Lower dimensional geometries are obtained by imposing restrictions to the angular neutronic flux. The XY (2D) geometry is obtained by imposing that the angular neutronic flux does not depend on the third coordinate, $\Phi = \Phi(x, y, \vec{\Omega})$, so $\frac{\partial \Phi}{\partial z} = 0$, and also must satisfy the symmetry relation $\Phi(\theta) = \Phi(\pi - \theta)$, so the moments $\phi_{lm} = 0$ if $l + m$ is odd (see the subsection on reflective boundary conditions). The planar (1D) geometry is obtained imposing that the neutronic flux $\Phi = \Phi(z, \theta)$ so the only nonzero moments are $\phi_{l,m=0} = \xi_{l0}$ and they are real.

2.1. Vacuum boundary conditions

When the region described by Eq. (1) is surrounded by vacuum, the angular neutronic flux at external surfaces is zero for every incoming direction,

$$\Phi(\vec{r}, \vec{\Omega}) = 0 \ , \qquad \text{for all } \vec{\Omega}\, \vec{n} \leq 0 \ , \tag{14}$$

where $\vec{n}$ is the outwardly directed unitary normal vector to the external surface. This condition can be approximated by setting Marshak's conditions (Stacey, 2001)

$$\int_{\vec{\Omega}\, \vec{n} \leq 0} d\vec{\Omega}\ Y_l^m(\vec{\Omega})^* \, \Phi(\vec{r}, \vec{\Omega}) = 0 \ , \tag{15}$$

for $l = 1, 3, 5, \ldots, L$ (odd) and $m = 0, 1, \ldots, l$ (the conditions with negative m index are redundant because the neutronic flux Φ is a real function). Notice that Eq. (15) is complex so there are $2l + 1$ real conditions for each index l odd.

We will only consider regions with prismatic geometry; we can then use the symmetry $Y_l^m(-\vec{\Omega}) = (-1)^l Y_l^m(\vec{\Omega})$ obtaining that, for $l + l'$ even,

$$\int_{\vec{\Omega}\, \vec{n} \leq 0} d\vec{\Omega}\ Y_l^m(\vec{\Omega})^* \, Y_{l'}^{m'}(\vec{\Omega}) = \frac{1}{2} \int d\vec{\Omega}\ Y_l^m(\vec{\Omega})^* \, Y_{l'}^{m'}(\vec{\Omega}) = \frac{1}{2} \delta_{ll'}\, \delta_{mm'} \, . \tag{16}$$

Inserting the expansion given by Eq. (2), truncated up to a finite odd order L, into Marshak's conditions (15) and using (16), it results into the conditions

$$
\begin{aligned}
\frac{1}{2}\phi_{lm} + \sum_{l' \text{ even}}^{L-1} \sum_{m'=-l'}^{l'} \left(\int_{\vec{\Omega}\,\vec{n}\leq 0} d\vec{\Omega}\; Y_l^m(\vec{\Omega})^*\, Y_{l'}^{m'}(\vec{\Omega}) \right) \phi_{l'm'} \\
= \frac{1}{2}\phi_{lm} + \sum_{l' \text{ even}}^{L-1} \Big[\int_{\vec{\Omega}\,\vec{n}\leq 0} d\vec{\Omega}\; Y_l^m(\vec{\Omega})^*\, Y_{l'}^0(\vec{\Omega})\, \phi_{l0} \\
+ \sum_{m'=1}^{l'} \int_{\vec{\Omega}\,\vec{n}\leq 0} d\vec{\Omega}\; Y_l^m(\vec{\Omega})^* \left(Y_{l'}^{m'}(\vec{\Omega})\, \phi_{l'm'} + Y_{l'}^{m'}(\vec{\Omega})^*\, \phi_{l'm'}^* \right) \Big] = 0 \ , \quad (17)
\end{aligned}
$$

for $l = 1, 3, 5, \ldots, L$ and $m = 0, 1, \ldots, l$. Taking real and imaginary part in Eq. (17), Marshak's conditions can be written as

$$
\bar{X} + N^V X = 0 \ , \qquad (18)
$$

where real vectors X and $\bar{X}$ were defined in previous section and N^V is a real rectangular matrix (of dimensions $n_o \times n_e$) whose numerical values depend on the geometry of the boundary surface, that is, the spatial axis normal to the boundary surface. For example, if the unitary normal vector $\vec{n}$ to the boundary surface points to negative Z axis, the integral

$$
\begin{aligned}
2\int_{\vec{\Omega}\,\vec{n}\leq 0} d\vec{\Omega}\; Y_l^m(\vec{\Omega})^*\, Y_{l'}^{m'}(\vec{\Omega}) = 2\int_0^{2\pi} d\varphi \int_0^{\pi/2} \sin\theta d\theta\; Y_l^m(\vec{\Omega})^*\, Y_{l'}^{m'}(\vec{\Omega}) \\
= 4\pi\delta_{mm'} \sqrt{\frac{2l+1}{4\pi}\frac{(l-m)!}{(l+m)!}} \sqrt{\frac{2l'+1}{4\pi}\frac{(l'-m)!}{(l'+m)!}} \int_0^1 d\mu\, P_l^m(\mu) P_{l'}^m(\mu) \ , \quad (19)
\end{aligned}
$$

($\mu = \cos\theta$) is real-valued and matrix N^V in Eq. (18), that will be denoted as N_3^{V-}, will have components given by Eq. (19). If vector $\vec{n}$ points to positive Z axis, the corresponding matrix $N_3^{V+} = -N_3^{V-}$ has opposite sign. Similar computations can be carried out for X and Y axis and the matrices $N_1^{V\pm}$, $N_2^{V\pm}$.

We finally observe that Marshak's conditions (15) depend on the order L of the angular approximation (see Equation (17)). Also, Equation (18) plays the role of "Fick's law" (12) at external surfaces, relating vector $\bar{X}$ with vector X.

2.2. Reflective boundary conditions

Reflective boundary conditions are applied at planes of symmetry. If physical conditions are equal at both sides, the neutronic flux must satisfy, at the symmetry plane,

$$\Phi(\vec{r},\vec{\Omega}) = \Phi(\vec{r},\tilde{\vec{\Omega}}) \ , \tag{20}$$

where $\tilde{\vec{\Omega}}$ is the reflected angular direction with respect to the symmetry plane. For example, if the normal vector $\vec{n}$ to the symmetry plane points to the negative Z axis, the symmetry condition is

$$\Phi(\vec{r},\varphi,\theta) = \Phi(\vec{r},\varphi,\pi-\theta) \ , \quad \text{for } 0<\varphi<2\pi \ , \ 0<\theta<\pi/2 \ . \tag{21}$$

Inserting expansion (2), this equation is equivalent to the following

$$\sum_{l=0}^{\infty}\sum_{m=-l}^{+l}(1-(-1)^{l+m})\,\phi_{lm}(\vec{r})\,Y_l^m(\vec{\Omega}) = 0 \ ,$$

that is,

$$\phi_{lm} = 0 \ , \qquad \text{whenever } l+m \text{ odd}, \tag{22}$$

for $l = 0,1,\ldots$ and $m = 0,1,\ldots,l$. Notice that this condition is the same for normal vector $\vec{n}$ pointing to the positive Z axis. It also corresponds to the XY symmetry for 2D geometry. In the particular case of 1D geometry, only $m=0$ moments are nonzero so the symmetry condition is $\phi_{l0}=0$ for l odd. If the spherical harmonics expansion (2) is truncated at finite order L then equations (22) form a set of $L(L+1)/2 = n_e$ conditions. We can reformulate condition (22) in matrix form by splitting vectors X and $\bar{X}$ in blocks that, symbolically, are

$$X = \begin{bmatrix} \phi_{l=\text{even},m=\text{even}} \\ \phi_{l=\text{even},m=\text{odd}} \end{bmatrix} \ , \qquad \bar{X} = \begin{bmatrix} \phi_{l=\text{odd},m=\text{even}} \\ \phi_{l=\text{odd},m=\text{odd}} \end{bmatrix} \ . \tag{23}$$

Then symmetry conditions (22) are equivalent to

$$N_3^R X = 0 \qquad \text{and} \qquad \bar{N}_3^R \bar{X} = 0 \ , \tag{24}$$

at the symmetry surface, where N_3^R is a square matrix of dimension $n_e \times n_e$ and $\bar{N}_3^R$ is a rectangular matrix of dimension $n_e \times n_o$ with the following block structure ($\mathbb{I}$ is the identity matrix)

$$N_3^R = \begin{bmatrix} 0 & 0 \\ 0 & \mathbb{I} \end{bmatrix} \ , \qquad \bar{N}_3^R = \begin{bmatrix} \mathbb{I} & 0 \\ 0 & 0 \end{bmatrix} \ .$$

In a similar fashion, reflective boundary conditions are computed when the normal vector to the symmetry surface points to X and Y axis, and are the following

$$\phi_{lm} - (-1)^m \phi_{lm}^* = \phi_{lm} - \phi_{l,-m} = 0 \ , \quad \text{for YZ symmetry surface,} \tag{25}$$
$$\phi_{lm} - \phi_{lm}^* = \phi_{lm} - (-1)^m \phi_{l,-m} = 0 \ , \quad \text{for XZ symmetry surface.} \tag{26}$$

2.3. Zero flux boundary conditions

If the boundary surface is far away from fission sources the angular neutronic flux is (almost) null $\Phi \simeq 0$ so zero flux approximation can be written as $X = 0$ and $\bar{X} = 0$ at external surfaces.

3. The nodal collocation method for an isotropic source

Since P_L equations (13) have a diffusive form, their spatial discretization can be done using a nodal collocation method, previously used for the neutron diffusion equation (Hébert, 1987; Verdú et al., 1994) and generalized for eigenvalue problems in multidimensional rectangular geometries (Capilla et al., 2005, 2008, 2012). We will only apply the method when the source term in Eq. (1) is isotropic because only this case will be treated in the numerical examples. This implies that $\bar{\mathcal{S}} = 0$ and no source term appears in Fick's law (12). This situation was studied in Capilla et al. (2012) so we will only briefly describe the method.

The first step to discretize the P_L equations is to divide the region where these equations have to be solved into N prismatic nodes of the form

$$\mathcal{N}^e = \prod_{j=1}^{3} [x_{j,m-\frac{1}{2}}, x_{j,m+\frac{1}{2}}] \, , \quad e = 1, \ldots, N \, .$$

For a generic node e the following change of variables

$$u_j = \frac{1}{\Delta x_j^e} \Big(x_j - \frac{1}{2} (x_{j,m-\frac{1}{2}} + x_{j,m+\frac{1}{2}}) \Big) \ , \tag{27}$$

where $\Delta x_j^e = x_{j,m+\frac{1}{2}} - x_{j,m-\frac{1}{2}}$, $j = 1, 2, 3$, transforms the node e into the cubic node $\mathcal{N}_u^e = [-1/2, +1/2]^3$ (of volume one).

The nodal collocation method assumes that on each node the nuclear cross-sections and the "effective" source term in Eq. (13) are constant. For each node e, Eq. (13) are transformed by means of the change of variables (27). Furthermore, if $X^e(u_1, u_2, u_3)$ denotes the previously defined vector of l even moments that appears in Eq. (13) for node e, it is assumed that vector X^e can be expanded in terms of (orthonormal) Legendre polynomials $\mathcal{P}_k(u)$ (Capilla et al., 2005) up to a certain finite order M,

$$X^e(u_1, u_2, u_3) = \sum_{k_1,k_2,k_3=0}^{M} x^e_{k_1k_2k_3} \mathcal{P}_{k_1}(u_1)\, \mathcal{P}_{k_2}(u_2)\, \mathcal{P}_{k_2}(u_3)\,, \tag{28}$$

where $u_j \in [-1/2, +1/2]$, $j = 1, 2, 3$. Notice that the polynomial expansion of the source term at node e, $\mathcal{S}^e_{\text{eff}}$, reduces to the constant term. The series (28) is then inserted into Eqs. (13) and equations for the Legendre moments $x^e_{k_1k_2k_3}$ are derived using the orthonormality properties of $\mathcal{P}_k(u)$.

Double derivative terms in Eqs. (13) will involve coupling with neighboring nodes. When node e is an interior node, adjacent nodes are related imposing continuity of the angular flux $\Phi(\vec{r}, \vec{\Omega})$ (or, equivalently, of all moments X^e and $\bar{X}^e$) at the interface between nodes. In the case that the node e is adjacent to a boundary then appropriate boundary conditions are used: Marshak's vacuum boundary conditions, reflective boundary conditions or zero flux boundary conditions.

Finally, once an appropriate ordering of the indices is chosen, the previous procedure approximates Eq. (13) by an algebraic problem that can be casted in the form

$$\mathcal{A}\, V = \mathcal{S}\,, \tag{29}$$

where V is a real vector of components $(\xi^e_{l,m\geq 0;k_1k_2k_3}, \eta^e_{l,m>0;k_1k_2k_3})$, $\mathcal{S}$ is the independent term associated with the source term and $\mathcal{A}$ is a matrix of dimension $N \times G \times N_{\text{Leg}} \times n_e$, where N is the number of nodes; G is the number of energy groups; $N_{\text{Leg}} = M^d$ is the number of Legendre moments, being M the order in Legendre series (28) and d the spatial dimension; and finally n_e is the number of components of vector X (i.e. the number of even l moments), being L the order of the P_L approximation.

Problem (29) is a system of linear equations that is large and sparse. The linear system is then iteratively solved using the bi-conjugate gradient stabilized method BCGSTAB, with incomplete LU factorization ILUT as preconditioner, from the FORTRAN library SPARSKIT (Saad, 1994).

4. Numerical results

The nodal collocation method developed in previous sections has been implemented into a multi-group code, SHNC (Spherical Harmonics Nodal Collocation) (Capilla et al., 2012), which solves the isotropic fixed source problem (1) for an arbitrary P_L approximation, with odd order L. In this Section, some calculations are presented to examine the accuracy and convergence of the method described above. In order to compare the different flux solutions obtained with the SHNC code to reference values in a spatial mesh of points x_i, we use the relative error $E_{r,i}$ and the maximum flux difference $E_{\max}$ defined by:

$$E_{r,i} = \frac{|\phi_i - \phi_i^{\text{ref}}|}{\phi_i^{\text{ref}}}\,, \qquad E_{\max} = \max_i (E_{r,i})\,,$$

where ϕ_i^{ref} is the reference scalar flux at point x_i.

4.1. One-dimensional source problem with vacuum boundary conditions

In order to validate the accuracy of the nodal collocation approach we analyse an academical test example consisting of a simple slab model of length l_x with fixed source and without scattering and fission. Vacuum boundary conditions are used at both outer boundaries (see Fig. 1). The corresponding problem for the neutron transport angular flux is

$$\begin{aligned}
&\mu \frac{d\Phi}{dx}(x,\mu) + \Sigma_t\,\Phi(x,\mu) = S\,, \quad 0 < x < l_x\,,\\
&\Phi(0,\mu) = 0\,, \quad \text{for } 0 < \mu \le +1\,,\\
&\Phi(l_x,\mu) = 0\,, \quad \text{for } -1 \le \mu < 0\,,
\end{aligned} \tag{30}$$

where $\mu = \cos\theta$. The analytical solution to this problem is easy to obtain. If $\mu \neq 0$ is kept fixed, the general solution of the first order ordinary differential equation is $\Phi(x,\mu) = C(\mu) e^{-\frac{\Sigma_t}{\mu}(x-\frac{l_x}{2})} + \frac{S}{\Sigma_t}$ where $C(\mu)$ is a function only of μ. If we impose the boundary conditions we get $C(\mu > 0) = -\frac{S}{\Sigma_t} e^{-\frac{\Sigma_t}{\mu}\frac{l_x}{2}}$ and $C(\mu < 0) = -\frac{S}{\Sigma_t} e^{+\frac{\Sigma_t}{\mu}\frac{l_x}{2}}$, so the solution of (30) is given by

$$\Phi(x,\mu) = \begin{cases} \frac{S}{\Sigma_t}\left(1 - e^{-\frac{\Sigma_t}{\mu}\left(x - \frac{l_x}{2} + \text{sgn}(\mu)\frac{l_x}{2}\right)}\right), & \text{if } \mu \neq 0\,,\\ \frac{S}{\Sigma_t}\,, \quad \text{if } \mu = 0\,, \end{cases} \tag{31}$$

where $\mathrm{sgn}(\mu) = \frac{\mu}{|\mu|}$. The scalar flux is then given by

$$\bar{\Phi}(x) = \frac{1}{2}\int_{-1}^{+1} d\mu\, \Phi(x,\mu) = \frac{S}{\Sigma_t}\left[1 - \frac{1}{2}\int_{0}^{1} d\mu \left(e^{-\frac{\Sigma_t}{\mu}x} + e^{-\frac{\Sigma_t}{\mu}(l_x - x)}\right)\right]. \quad (32)$$

We have chosen this example because, due to its particular geometry, the classical diffusion and the P_1 approximation do not provide good result and it is necessary to use higher approximations to the transport equation.

We have calculated the numerical P_L solutions for the fluxes with the SHNC code for the slab in Fig. 1 of length $l_x = 1$ cm. The total cross-section considered is $\Sigma_t = 1$ cm^{-1}, and the homogeneous isotropic neutron source has strength $S = 1$ n/cm^2 s. The size of the spatial nodes is 0.1 cm and the order of the Legendre polynomials considered is $M = 5$. Also, we have solved exactly the P_L equations (13) for this problem by using a symbolic computational software program (Wolfram Research Inc., 2010). We have found that, from $L = 1$ to $L = 25$, the exact results of the P_L equations coincide with the numerical SHNC solutions.

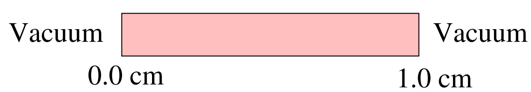

Figure 1: Geometry of the one-dimensional problem with vacuum boundary conditions.

The scalar fluxes are given in Table 1 for $P_1 - P_7$, P_{15} and P_{25} approximations, together with the analytical transport solution (32), obtained by numerical integration using Quadpack (Piessens et al., 1983), for $0\,\mathrm{cm} \leq x \leq 0.5\,\mathrm{cm}$. Table 1 also shows the maximum flux differences ($E_{\max}$) of the P_L results as compared to the reference transport solutions. It is seen that the fluxes obtained by the P_L approximations converge to the exact value as the order L of the approximation increases.

We observe that the maximum error of scalar flux for the P_1 approximation amounts to 10.40% at $x = 0.3$ cm. As we have commented above, P_1 equation does not provide a good approximation to the transport equation. However, the maximum error decreases as the order L of the P_L approximation increases. When $L > 1$ the maximum differences amount at the slab boundary ($x = 0$ cm), where Marshak's approximation to vacuum boundary condition occurs.

Table 1: Scalar fluxes for the homogeneous slab with vacuum boundary conditions

	SHNC - Order of approximations						
x (cm)	P_1	P_3	P_5	P_7	P_{15}	P_{25}	Transport
0.0	0.44676	0.45104	0.44315	0.43815	0.43169	0.42951	0.42575
0.1	0.50579	0.53489	0.53977	0.54248	0.54957	0.55230	0.55252
0.2	0.54996	0.59437	0.60428	0.60823	0.61286	0.61299	0.61247
0.3	0.58059	0.63395	0.64527	0.64829	0.64880	0.64812	0.64797
0.4	0.59861	0.65658	0.66798	0.66991	0.66780	0.66717	0.66722
0.5	0.60456	0.66394	0.67526	0.67674	0.67379	0.67326	0.67336
$E_{\max}$ (%)	10.40	5.93	4.10	2.92	1.40	0.88	

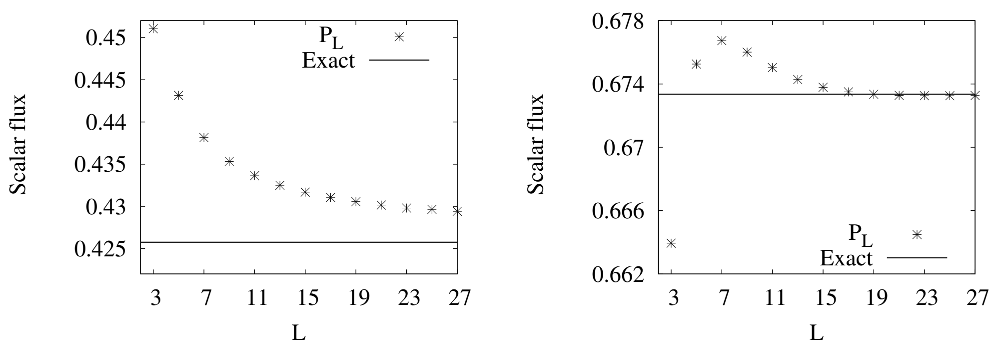

Figure 2: Scalar fluxes at $x = 0$ cm (left) and $x = 0.5$ cm (right) from P_L approximations ($L = 3, ..., 27$) and the transport solution (horizontal line).

The graphics in Fig. 2 show the scalar fluxes at the left boundary ($x = 0$ cm) and at the center of the slab ($x = 0.5$ cm) for successive P_L approximations from $L = 3$ to $L = 27$ (odd L). In both cases the P_L fluxes are compared to the exact transport solution (horizontal line) at the same point. It is observed that the convergence of the P_L solution to the analytical value is very slow at $x = 0$ cm, and there are no appreciable changes for $L \geq 23$, while in the center of the slab, at $x = 0.5$ cm the convergence is much faster.

We graphically illustrate the previous comments in Fig. 3, where we show the scalar fluxes for the $P_1 - P_9$ approximations, together with the analytical transport solution.

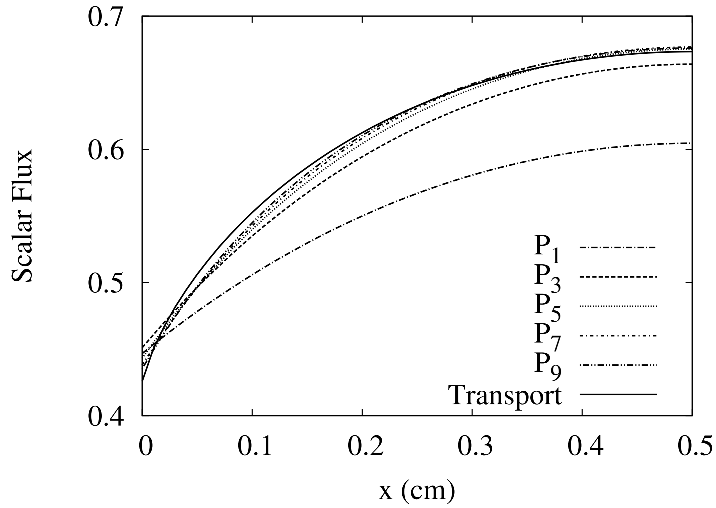

Figure 3: Scalar fluxes for the homogeneous slab problem.

4.2. Two-region source problem with reflective boundary conditions

Let us consider a one-dimensional two-region slab with lengths l_{x1} and $l_{x2} - l_{x1}$ for region 1 and region 2 respectively, without scattering and fission. Reflective boundary conditions are considered at both outer boundaries. Only region 1 has a fixed source S.

The analytical description of the problem is as follows:

$$\begin{aligned} &\mu \frac{d\Phi}{dx}(x,\mu) + \Sigma_t \, \Phi(x,\mu) = \begin{cases} S\,, & 0 < x < l_{x1}\,, \\ 0\,, & l_{x1} < x < l_{x2}\,, \end{cases} \\ &\Phi(0, \mu > 0) = \Phi(0, \mu < 0)\,, \\ &\Phi(l_{x2}, \mu > 0) = \Phi(l_{x2}, \mu < 0)\,. \end{aligned} \tag{33}$$

Proceeding as is previous subsection, if $\mu \neq 0$ is kept fixed, the general solution of the first order differential equation at region 1 is $\Phi^1(x,\mu) = C^1(\mu) e^{-\frac{\Sigma_t}{\mu} x} + \frac{S}{\Sigma_t}$ $(0 < x < l_{x1})$ and at region 2 is $\Phi^2(x,\mu) = C^2(\mu) e^{-\frac{\Sigma_t}{\mu} x}$ $(l_{x1} < x < l_{x2})$. The functions $C^1(\mu)$ and $C^2(\mu)$ are then determined by imposing continuity of the solution at $x = l_{x1}$ and reflective boundary conditions at $x = 0$ and $x = l_{x2}$. The solution is then

$$\Phi(x,\mu) = \begin{cases} \dfrac{S}{\Sigma_t}\left(1 - \dfrac{\sinh \frac{\Sigma_t}{\mu}(l_{x2} - l_{x1})}{\sinh \frac{\Sigma_t}{\mu} l_{x2}}\, e^{-\frac{\Sigma_t}{\mu}x}\right), & 0 < x < l_{x1}\,, \\ \dfrac{S}{\Sigma_t} \dfrac{\sinh \frac{\Sigma_t}{\mu} l_{x1}}{\sinh \frac{\Sigma_t}{\mu} l_{x2}}\, e^{\frac{\Sigma_t}{\mu}(l_{x2}-x)}\,, & l_{x1} < x < l_{x2}\,, \end{cases} \tag{34}$$

and the corresponding scalar flux is

$$\bar{\Phi}(x) = \begin{cases} \dfrac{S}{\Sigma_t}\left(1 - \displaystyle\int_0^1 d\mu\, \dfrac{\sinh \frac{\Sigma_t}{\mu}(l_{x2} - l_{x1})}{\sinh \frac{\Sigma_t}{\mu} l_{x2}} \cosh \dfrac{\Sigma_t}{\mu} x\right), & 0 < x < l_{x1}\,, \\ \dfrac{S}{\Sigma_t} \displaystyle\int_0^1 d\mu\, \dfrac{\sinh \frac{\Sigma_t}{\mu} l_{x1}}{\sinh \frac{\Sigma_t}{\mu} l_{x2}} \cosh \dfrac{\Sigma_t}{\mu}(l_{x2} - x)\,, & l_{x1} < x < l_{x2}\,. \end{cases} \tag{35}$$

We have computed numerical results when the length of each region is $l_{x1} = l_{x2} - l_{x1} = 1$ cm, as it is shown in Fig. 4. The total cross-section in region 1 is $\Sigma_t = 1$ cm^{-1} and there is a source of strength $S = 1$ n/cm^2 s. The cross-section of region 2 is the same as that of region 1, except having no fixed source. The SHNC calculation was performed using a mesh size of 0.1 cm and a Legendre polynomial order of $M = 5$.

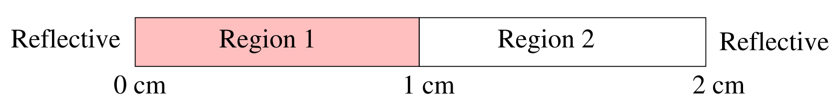

Figure 4: Geometry of two regions for the slab problem with reflective boundary conditions.

In Table 2 the scalar fluxes for $P_1 - P_9$, and P_{15} approximations are compared with the analytical transport solution (35) for $0\,\text{cm} \le x \le 2\,\text{cm}$. The Table also shows the maximum flux differences.

We observe that for this problem, the P_L scalar fluxes for $L \ge 3$ at the slab boundaries are closer to the transport solutions than in the previous example, because reflective boundary conditions are incorporated into P_L equations in an exact way. In Fig. 5 we have plotted the P_L scalar fluxes for $L = 1, 3, 5, 7$ and the exact transport solution.

Table 2: Scalar fluxes for the two-region problem with reflective boundary conditions

	SHNC - Order of approximations						
x (cm)	P_1	P_3	P_5	P_7	P_9	P_{15}	Transport
0.0	0.82845	0.86648	0.86462	0.86228	0.86138	0.86117	0.86124
0.4	0.78560	0.82895	0.83291	0.83261	0.83198	0.83105	0.83096
0.8	0.63566	0.67265	0.68727	0.69498	0.69927	0.70373	0.70368
1.2	0.36434	0.32735	0.31273	0.30502	0.30073	0.29627	0.29631
1.6	0.21440	0.17105	0.16710	0.16739	0.16802	0.16895	0.16904
2.0	0.17155	0.13352	0.13538	0.13772	0.13862	0.13883	0.13876
$E_{\max}$ (%)	26.83	10.49	5.53	2.93	1.48	0.03	

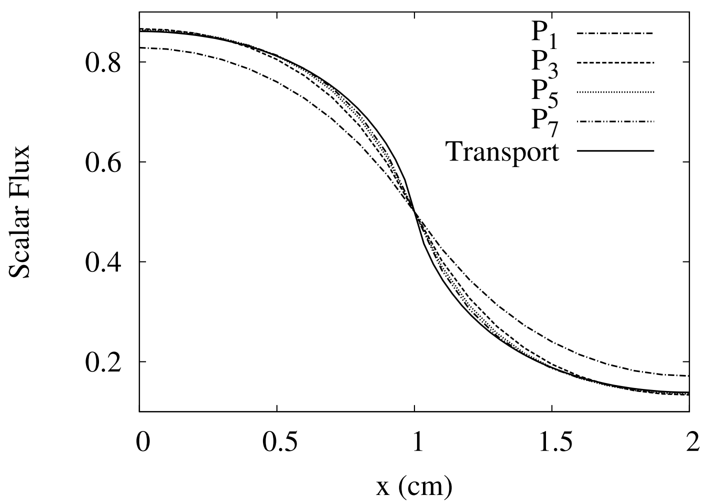

Figure 5: Scalar fluxes for the two-region slab problem.

4.3. Two-group anisotropic scattering problem

In this Section we consider the one-dimensional two-region two-group source problem with P_3 scattering which was defined by Roy (1991) and also presented in Ju et al. (2007). The geometry of this problem is shown in Fig. 6, there is a source region and homogeneous cross-sections as given in Table 3 for region 1. The cross-sections of region 2 are the same as that of region 1, except having no fixed source. The boundary condition is reflective at $x = 0.0$ cm and vacuum at $x = 20.0$ cm.

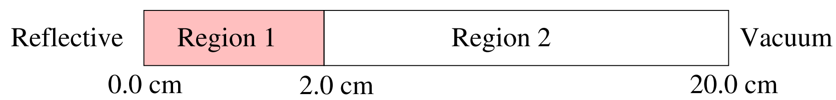

Figure 6: Geometry of two regions for anisotropic scattering problem.

Table 3: Cross-section and source strength data in the region 1 for the anisotropic scattering problem

Group	Source	Total	$\Sigma_{s,g\to g}$ (cm^{-1})				$\Sigma_{s,g\to g+1}$(cm^{-1})			
g	S (n/cm^2 s)	Σ_t (cm^{-1})	Σ_s^0	Σ_s^1	Σ_s^2	Σ_s^3	Σ_s^0	Σ_s^1	Σ_s^2	Σ_s^3
1	1	1	0.5	0.3	0.2	3/35	0.5	0.3	0.2	3/35
2	1	1	0.5	0.3	0.2	3/35	-	-	-	-

The group 1 and group 2 scalar fluxes for $P_1 - P_7$ approximations obtained by the SHNC code are given in Tables 4 and 5 respectively, at the beginning of the source region, at the end of the scattering region and at the interface of the two regions. The mesh size considered is 0.5 cm and the polynomial order is $M = 5$. In Tables 4 and 5, we also compare the results obtained with our code with the results obtained by an ANISN reference calculation on 320 meshes (Riyait and Ackroyd, 1987).

If Figs. 7(a) and 7(b), we show the $P_1 - P_7$ scalar flux solutions for group 1 and 2, respectively.

4.4. Two-dimensional problem with vacuum boundary conditions

This problem is a one-group three-region fixed source problem. The geometry of the system is a $[0, 100] \times [0, 100]$ square domain with a unit isotropic source located in $[0, 10] \times [0, 10]$, as can be seen in Fig. 8. The boundary conditions are reflective at $x = 0$ cm, $y = 0$ cm; and vacuum at $x = 100$ cm and $y = 100$ cm. There is no scattering and fission, and the total cross-section data are also shown in Fig. 8. The geometry of this problem has been inspired by the one-group 3D benchmark problem 1, see Kobayashi (1997); Ackroyd and Riyait (1989), which is collapsed to a two-dimensional benchmark. We have modified the total cross-section of the material in region 2, which corresponds to the void region in the Kobayashi's Problem 1. It is well

Table 4: Group 1 scalar fluxes for the P_3 scattering problem

	SHNC				
x (cm)	P_1	P_3	P_5	P_7	ANISN ref.
0.125	1.74026	1.76552	1.75996	1.75941	1.75949
0.375	1.72312	1.75290	1.74791	1.74710	1.74706
1.875	1.10136	1.13464	1.15398	1.16467	1.16971
2.125	0.86518	0.82028	0.80103	0.79040	0.78535
2.375	0.66966	0.58981	0.56594	0.55805	0.55585
2.625	0.51832	0.43529	0.42041	0.41856	0.41958
18.875	3.03740E−8	7.24444E−7	7.80904E−7	7.80953E−7	7.77495E−7
19.125	2.34905E−8	5.90130E−7	6.38380E−7	6.38505E−7	6.35673E−7
19.375	1.81571E−8	4.78667E−7	5.20218E−7	5.20433E−7	5.18211E−7
19.625	1.40217E−8	3.85037E−7	4.21239E−7	4.21458E−7	4.19663E−7
19.875	1.08116E−8	3.04538E−7	3.36283E−7	3.35723E−7	3.33956E−7

Table 5: Group 2 scalar fluxes for the P_3 scattering problem

	SHNC				
x (cm)	P_1	P_3	P_5	P_7	ANISN ref.
0.125	3.21648	3.30634	3.29655	3.29514	3.20460
0.375	3.18201	3.27793	3.26988	3.26815	3.17762
1.875	2.10894	2.15417	2.17954	2.19316	2.16312
2.125	1.75585	1.68801	1.66223	1.64877	1.64672
2.375	1.44481	1.31391	1.27674	1.26456	1.29081
2.625	1.18469	1.03456	1.00694	1.00267	1.04638
18.875	3.21510E−7	4.93422E−6	5.17357E−6	5.17240E−6	7.21376E−6
19.125	2.51255E−7	4.04638E−6	4.25508E−6	4.25451E−6	5.95205E−6
19.375	1.96019E−7	3.29851E−6	3.48230E−6	3.48275E−6	4.89303E−6
19.625	1.52514E−7	2.65925E−6	2.82270E−6	2.82404E−6	3.99218E−6
19.875	1.18141E−7	2.09811E−6	2.24127E−6	2.23850E−6	3.19123E−6

known (de Oliveira et al., 2001) that codes based on angular approximations of the transport equation have difficulties in the convergence when dealing with problems that involve void regions.

Table 6 contains the scalar fluxes along $y = 5$, for 5 cm $\leq x \leq$ 95 cm, obtained by SHNC from the nodal collocation method for the P_L ($L =$

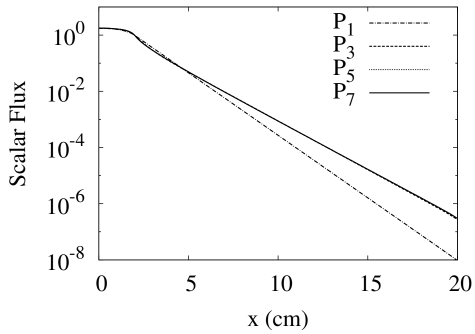

(a) Group 1 scalar flux

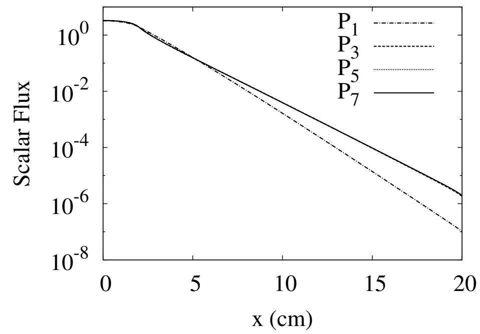

(b) Group 2 scalar flux

Figure 7: Scalar fluxes for the anisotropic P_3 scattering test case (logarithmic scale).

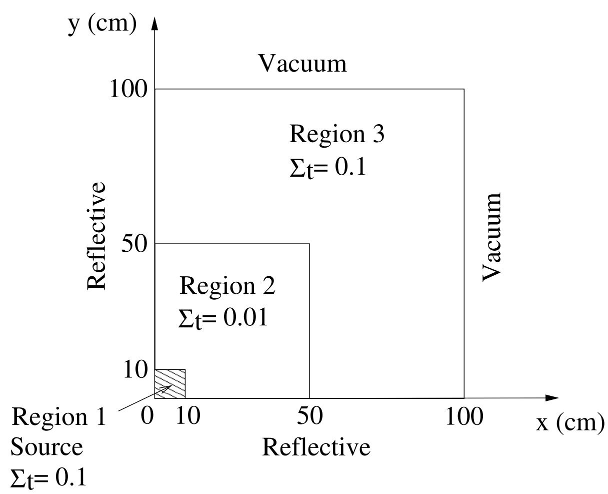

Figure 8: Geometry and cross-sections of 2D problem.

$1, 3, 9, 11$) approximations. We have considered 20×20 nodes with side length 5 cm and $M = 3$ polynomials in the nodal expansion. The Table also shows reference results for the mean scalar fluxes calculated by the S_N code TWODANT (Alcouffe et al., 1995) ($N = 16$), with 600×600 mesh points and a convergence criterion of 10^{-7}.

The results for this problem show that it is necessary to consider a high order L in the P_L approximation, to obtain good convergence of the total

Table 6: Scalar fluxes along $y = 5$ cm for the two-dimensional problem with vacuum boundary conditions

	SHNC - Order of approximations				
x (cm)	P_1	P_3	P_9	P_{11}	S_{16} ref.
5	4.92451	5.91080	6.65538	6.75852	6.7754
15	1.76186	2.28857	2.47655	2.37419	2.0977
25	1.27221	1.51094	1.16018	1.03506	1.0202
35	9.72670E−1	1.03561	5.95950E−1	5.90657E−1	6.2759E−1
45	7.77691E−1	6.83954E−1	4.67358E−1	5.02396E−1	3.9092E−1
55	2.97616E−1	2.14824E−1	1.90635E−1	1.78891E−1	1.3633E−1
65	5.18661E−2	5.20840E−2	4.68202E−2	4.51401E−2	3.2807E−2
75	9.04519E−3	1.50128E−2	1.28345E−2	1.26740E−2	1.0172E−2
85	1.57869E−3	4.50248E−3	3.76739E−3	3.68766E−3	3.1774E−3
95	2.78968E−4	1.35659E−3	1.14070E−3	1.10019E−3	1.0390E−3

flux. The relative error of the P_{11} scalar flux at the source region ($x = y = 5$ cm) is $E_r = 0.24\%$. We observe that this high order of approximation $L = 11$ introduces oscillating behaviour due to the polynomial nature of the approximation.

Fig. 9 shows comparisons between the S_{16} mean scalar flux and the P_L fluxes for $L = 1, 3, 5, 11$ along the line $y = 5$ cm. The S_{16} results are drawn in as reference, and we observe convergence of the P_L fluxes toward the S_{16} solution.

Also, we have replaced the vacuum boundary adding purely absorbing material of thickness 50 cm, with $\Sigma_t = 1$ cm^{-1}, around the object and setting zero flux conditions at $x = 150$ cm and $y = 150$ cm. The results at the squared region $[0, 100] \times [0, 100]$ are exactly the same than the ones obtained with vacuum conditions.

4.5. Fletcher's problem

We consider now the one-group source problem presented by Fletcher (1981, 1983) and also studied in Kobayashi et al. (1986). The system consists of a square of pure absorber, whose side length is 4 cm and it includes a neutron source of strength $S = 1/1.44$, in a square of $(1.2\,\mathrm{cm})^2$, as shown in Fig. 10. The source gives a strength of unit when integrated over the source region. The system is homogeneous with $\Sigma_t = \Sigma_a = 1$ cm^{-1}, there is no scattering so that the exact solution becomes an integral of exponential

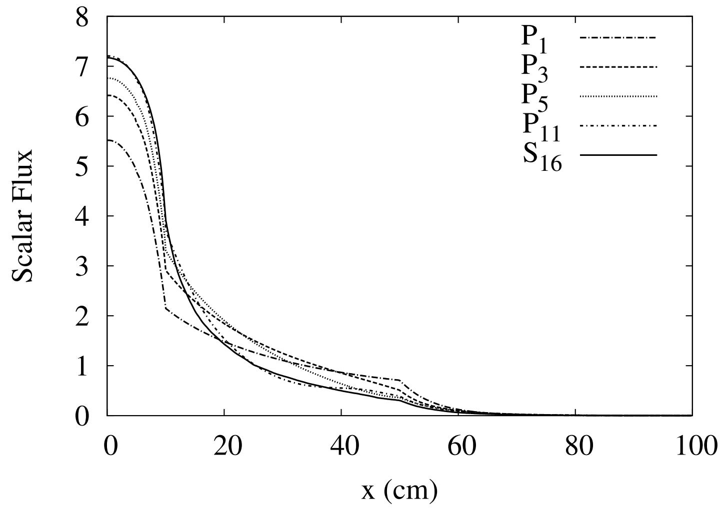

Figure 9: Scalar fluxes along the line $y = 5$ cm for the 2D one-group problem.

terms over the source region (Fletcher, 1981). The boundary conditions are reflective at $x = 0$ cm and $y = 0$ cm, and vacuum boundary conditions are simulated at $x = 4$ cm and $y = 4$ cm, by replacing the surfaces with purely absorbing material, of thickness 3 cm, around the system and setting zero flux conditions at $x = 7$ cm and $y = 7$ cm.

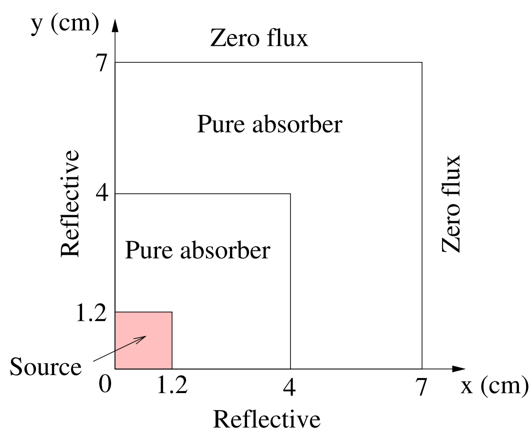

Figure 10: Geometry of Fletcher's problem.

To solve this problem we have considered a mesh width of 0.2 cm in X and Y directions and the order of the Legendre polynomials in the expansions of $M = 5$. The total flux along the line $y = 3.9$ cm (0.1 cm from the $x = 4$ boundary) obtained by the SHNC code, is given in Table 7 for the $P_1 - P_7$ approximations together with the exact calculation given by Fletcher (1983), taken as reference. We observe that the P_7 results are close to the exact result. The maximum differences of scalar flux as compared to the reference value are 0.93% at $x = 0.5$ cm for the P_5 approximation, and 0.32% at $x = 1.9$ cm for the P_7 approximation, so the SHNC results agree well with the reference solution.

Table 7: Scalar flux along the line $y = 3.9$ cm for Fletcher's problem

	SHNC - Order of approximations				
x (cm)	P_1	P_3	P_5	P_7	Exact
0.1	1.92105E−3	2.52483E−3	2.62656E−3	2.60223E−3	2.6033E−3
0.3	1.88930E−3	2.49349E−3	2.59248E−3	2.56841E−3	2.5691E−3
0.5	1.82735E−3	2.43208E−3	2.52576E−3	2.50215E−3	2.5025E−3
0.7	1.73819E−3	2.34306E−3	2.42916E−3	2.40617E−3	2.4083E−3
0.9	1.62609E−3	2.22994E−3	2.30663E−3	2.28431E−3	2.2863E−3
1.1	1.49624E−3	2.09703E−3	2.16299E−3	2.14139E−3	2.1438E−3
1.3	1.35440E−3	1.94919E−3	2.00367E−3	1.98291E−3	1.9858E−3
1.5	1.20643E−3	1.79148E−3	1.83428E−3	1.81467E−3	1.8180E−3
1.7	1.05793E−3	1.62886E−3	1.66031E−3	1.64226E−3	1.6460E−3
1.9	9.13775E−4	1.46590E−3	1.48679E−3	1.47064E−3	1.4754E−3
2.1	7.77925E−4	1.30657E−3	1.31802E−3	1.30403E−3	1.3076E−3
2.3	6.53243E−4	1.15408E−3	1.15746E−3	1.14574E−3	1.1490E−3
2.5	5.41506E−4	1.01085E−3	1.00765E−3	9.98188E−4	1.0007E−3
2.7	4.43499E−4	8.78534E−4	8.70275E−4	8.62912E−4	8.6523E−4
2.9	3.59184E−4	7.58075E−4	7.46199E−4	7.40700E−4	7.4261E−4
3.1	2.87903E−4	6.49824E−4	6.35635E−4	6.31710E−4	6.3350E−4
3.3	2.28580E−4	5.53655E−4	5.38275E−4	5.35629E−4	5.3694E−4
3.5	1.79901E−4	4.69091E−4	4.53430E−4	4.51785E−4	4.5285E−4
3.7	1.40459E−4	3.95402E−4	3.80167E−4	3.79276E−4	3.8026E−4
3.9	1.08865E−4	3.31708E−4	3.17411E−4	3.17059E−4	3.1793E−4

Fig. 11 shows the scalar fluxes along the line $y = 3.9$ cm of Table 7. The Figure also shows good convergence of the scalar flux as the order of the P_L approximation increases.

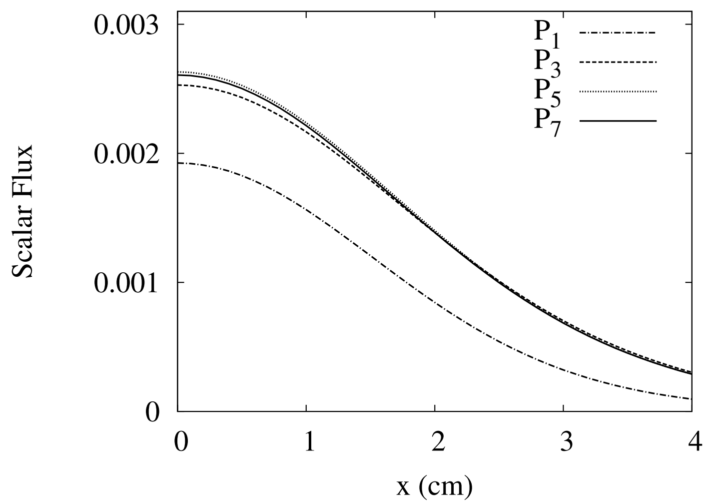

Figure 11: Scalar fluxes along the line $y = 3.9$ cm for Fletcher's problem.

4.6. Three-dimensional two-region fixed source problem

We now consider a one-group two-region problem. The three-dimensional system consists of a medium of uniform cross-section without scattering and fission. Fig. 12 shows the $x - z$ or $y - z$ plane geometry and dimensions of the two regions. There is a neutron source of strength $S = 1$ n/cm^2 s in region 1 of side length 10 cm. The total cross-section of region 1 and region 2 is $\Sigma_t = 0.1$ cm^{-1}. Reflective boundary conditions are used on planes $x = 0$, $y = 0$, $z = 0$, and vacuum boundary conditions on all outer boundaries.

We have performed the SHNC calculations for this problem using a mesh size of 5 cm, which corresponds to 20 nodes in each X, Y and Z direction, resulting in a total of $20^3 = 8000$ cubic nodes. Also a Legendre polynomial order of $M = 3$ is considered. In Table 8 we present the SHNC P_L solutions, $L = 1, 3, 5, 7$, for the total fluxes along $y = z = 5$ cm for 5 cm $\leq x \leq 95$ cm. These numerical results are compared against the mean scalar fluxes calculated with THREEDANT (Alcouffe et al., 1995), obtained using the S_{16} quadrature set, with $153 \times 153 \times 153$ spatial mesh and a convergence criterion of 10^{-7}.

Fig. 13 shows the scalar fluxes along $y = z = 5$ for successive SHNC P_L approximations ($L = 1, 3, 5$) in comparison with the S_{16} reference solution.

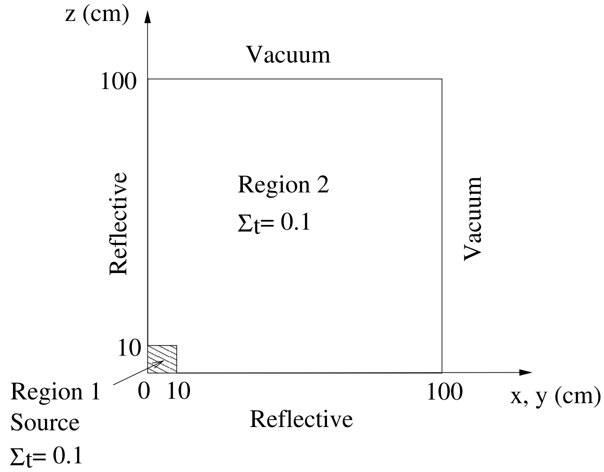

Figure 12: Geometry of 3D two-region problem.

Table 8: Scalar fluxes along $y = z = 5$ cm for 3D two-region source problem

x (cm)	SHNC - Order of approximations P_1	P_3	P_5	P_7	S_{16} ref.
5	4.80364	5.72341	5.95788	6.02348	5.9590
15	9.87415E−1	8.31685E−1	7.47349E−1	7.12514E−1	6.9432E−1
25	1.23928E−1	9.26805E−2	9.72075E−2	1.00976E−1	9.2191E−2
35	1.69588E−2	1.81047E−2	1.91493E−2	1.93783E−2	2.0887E−2
45	2.43752E−3	4.32946E−3	4.29474E−3	4.38193E−3	5.5191E−3
55	3.62431E−4	1.11162E−3	1.04748E−3	1.09268E−3	9.6625E−4
65	5.52422E−5	2.95739E−4	2.73205E−4	2.89897E−4	1.0581E−4
75	8.57975E−6	8.05365E−5	7.51786E−5	8.06746E−5	3.5413E−5
85	1.35258E−6	2.23331E−5	2.15506E−5	2.39287E−5	1.2941E−5
95	2.18613E−7	6.24834E−6	6.25460E−6	9.28789E−6	4.9319E−6

4.7. Three-dimensional three-region source problem

We consider a one-group source problem of simple geometry consisting of three regions, which is an extension to three dimensions of the two-dimensional problem presented in Section 4.4. The $x - z$ or $y - z$ plane geometry and dimensions of the three regions are the same as that shown in Fig. 8. There is a neutron source of strength $S = 1$ n/cm^2 s in region 1, the

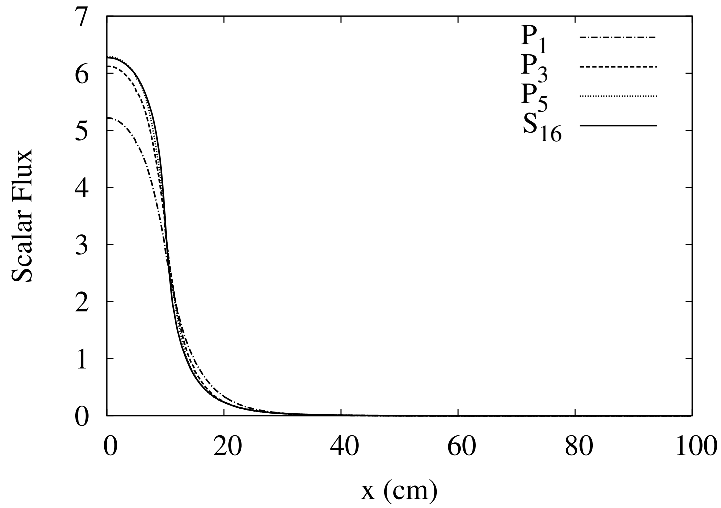

Figure 13: Scalar fluxes along $y = z = 5$ for 3D two-region source problem.

total cross-section of regions 1 and 3 is $\Sigma_t = 0.1$ cm^{-1}, and $\Sigma_t = 0.01$ cm^{-1} in region 2. There is no scattering and fission.

The SHNC P_L solutions for the fluxes have been calculated considering the same spatial discretization and Legendre polynomial order as in the previous 3D two-region problem. Also the same data are considered for the S_{16} calculations with THREEDANT code. Table 9 shows a comparison between P_L for $(L = 1, 3, 9, 11)$ and S_{16} fluxes along $y = z = 5$ cm. Comparison of the solutions is also made with the results obtained using the Monte-Carlo code MCNP (Los Alamos Scientific Laboratory, 1979).

A high order L is necessary to obtain convergence of the P_L fluxes, as it was observed in previous examples with similar geometry and the same boundary conditions (Sections 4.4 and 4.6). The relative errors of the scalar flux at the source region ($x = y = z = 5$ cm) are 2.31% and 1.95% for the P_{11} approximation, as compared to the MCNP and S_{16} results respectively.

Fig. 14 shows the scalar fluxes along $y = z = 5$ cm for successive SHNC P_L approximations $(L = 1, 3, 5, 11)$ in comparison with the S_{16} solution.

As we did in the 2D three-region problem (Section 4.4), we have simulated the vacuum boundary conditions at surfaces $x = 100$, $y = 100$, $z = 100$ by adding a purely absorbing material of thickness 50 cm, and $\Sigma_t = 1$ cm^{-1}, around the system and setting zero flux conditions at the new boundaries

Table 9: Scalar fluxes along $y = z = 5$ cm for 3D three-region source problem

x (cm)	SHNC - Order of approximations P_1	P_3	P_9	P_{11}	MCNP	S_{16}
5	3.44437	4.36675	5.58991	5.84245	5.98076	5.9590
15	6.88250E−1	1.17382	1.71573	1.66336	1.27906	1.2777
25	3.89167E−1	6.41086E−1	5.60190E−1	3.95420E−1	4.23722E−1	4.1510E−1
35	2.56074E−1	3.96101E−1	1.18969E−1	1.03104E−1	1.94155E−1	2.2288E−1
45	1.89093E−1	2.36820E−1	1.26421E−1	1.92404E−1	1.04966E−1	1.4463E−1
55	7.06794E−2	6.27775E−2	5.38342E−2	4.68457E−2	3.96974E−2	3.9059E−2
65	1.20454E−2	1.47703E−2	1.24652E−2	1.11190E−2	1.02486E−2	3.9734E−3
75	2.05824E−3	4.06631E−3	3.21621E−3	3.15692E−3	2.79712E−3	1.3628E−3
85	3.52479E−4	1.16671E−3	9.46793E−4	9.49270E−4	7.94589E−4	4.9627E−4
95	6.12108E−5	3.37607E−4	3.73524E−4	3.37575E−4	2.32674E−4	1.8460E−4

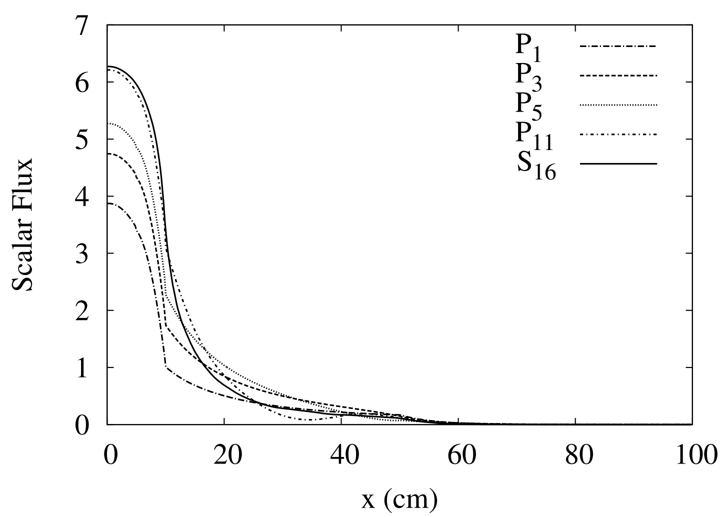

Figure 14: Scalar fluxes along $y = z = 5$ for 3D three-region source problem.

$x = 150$, $y = 150$, $z = 150$. Again, the results for the P_L fluxes are exactly the same than the ones obtained with vacuum conditions.

5. Conclusions

We have developed a diffusive approximation for the P_L spherical harmonics form of the source transport equation. The P_L diffusion equations have been implemented using the nodal collocation method in the computer code SHNC (Spherical Harmonics Nodal Collocation). While the zero and reflective flux boundary conditions are exact, the vacuum boundary condition requires an approximation. In the applications it is shown that Marshak's approximation to the vacuum boundary conditions is exactly the same that adding a purely absorbing medium with a sufficient thickness and setting the exactly zero flux condition at the new boundary.

This method has been applied to several 1D, 2D and 3D problems with an isotropic fixed source and with isotropic and anisotropic scattering, comparing the obtained results with the ones provided by several methods and codes: analytical and ANISN for 1D problems, TWODANT for 2D problems and THREEDANT and MCNP for 3D problems. The problems selected are chosen to test the new SHNC code in limit conditions, showing that in some cases it is necessary a high order L of the P_L spherical harmonics approximation, which works very well in non-scattering regions, but the P_L diffusive approximation has difficulties in the convergence when dealing with problems that involve void regions due to the presence of a cross-section term in the denominator of the leakage operator.

In one dimension the accuracy and convergence of the method has been validated with two source problems with analytical solution and, due to their geometry, requiring high order P_L approximation to the transport equation. The effect on convergence given by Marshak's approximation to vacuum boundary conditions has been clarified and compared with reflective (exact) boundary conditions. The code has also been applied to a two-region two-group source problem with anisotropic scattering due to Roy and results are in good agreement with reference calculations. We have then considered two and three-dimensional problems inspired by Kobayashi benchmark problems that require a high order P_L approximation to obtain accurate results.

Although the development of the paper is for the neutron transport equation, the treatment is also valid for the radiative transport equation.

Acknowledgements

This work has been partially supported by the Spanish Ministerio de Economía y Competitividad under project ENE2011-22823, and the Generalitat Valènciana under project PROMETEO11/2014/008.

References

Ackroyd, R. T., Riyait, N. S., 1989. Iteration and extrapolation method for the approximate solution of the even-parity transport equation for the systems with voids. Ann. Nucl. Energy, 16(1):1-32.

Alcouffe, R. E., Baker, R. S., Brinkley, F. W., Marr, D. R., O'Dell, R. D., Walters, W. F, 1995. DANTSYS: A diffusion accelerated neutral particle transport code system. Los Alamos National Laboratory, LA-12969-M.

Aydin, E. D., Katsimichas, S., de Oliveira, C. R. E., 2005. Time-dependent diffusion and transport calculations using a finite-element-spherical harmonics method. J. Quant. Spectrosc. Radiat. Transf., 95:349-363.

Capilla, M., Talavera, C. F., Ginestar, D., Verdú, G., 2005. A nodal collocation method for the calculation of the lambda modes of the P_L equations. Ann. Nucl. Energ., 32:1825-1853.

Capilla, M., Talavera, C. F., Ginestar, D., Verdú, G., 2008. A nodal collocation approximation for the multidimensional P_L equations - 2D applications. Ann. Nucl. Energ., 35:1820-1830.

Capilla, M., Talavera, C. F., Ginestar, D., Verdú, G., 2012. Application of a nodal collocation approximation for the multidimensional P_L equations to the 3D Takeda benchmark problems. Ann. Nucl. Energ., 40:1-13.

Courant, R., Hilbert, D., 1962. Methods of Mathematical Physics, Vol. I. Wiley-Interscience.

de Oliveira, C. R. E., Eaton, M. D., Umpleby, A. P., Pain, C. C., 2001. Finite element-spherical harmonics solutions of the 3D Kobayashi benchmarks with ray-tracing void treatment. Prog. Nucl. Energy, 39 (2):243-261.

Fletcher, J. K., 1981. Proc. Int. top. Mtg on Advances in Mathematical Methods for the Solution of Nuclear Engineering Problems, Munich, Vol. 1:17-36.

Fletcher, J. K., 1983. A solution of the neutron transport equation using spherical harmonics. J. Phys. A: Math. Gen., 16:2827-2835.

Gelbard, E. M., 1968. Spherical harmonics methods: P_L and double P_L approximations. Computing Methods in Reactor Physics. Kelberg, D., Okrent, C. N. (eds.). Gordon and Breach, New York.

Hébert, A., 1987. Development of the nodal collocation method for solving the neutron diffusion equation. Ann. Nucl. Energ., 14(10):527-541.

Ju, H. T., Wu, H. C., Zhou, Y. Q., Cao, L. Z., Yao, D., Xian, C. Y., 2007. A least-squares finite-element S_n method for solving first order neutron transport equation. Nucl. Eng. and Design, 237:823-829.

Kobayashi, K., Oigawa, H., Yamagata, H., 1986. The spherical harmonics method for the multigroup transport equation in $x - y$ geometry. Ann. Nucl. Energy, 13(12):663-678.

Kobayashi, K., 1997. A proposal for 3-D radiation transport benchmarks for simple geometries with void region, 3-D deterministic radiation transport computer programs. OECD Proceedings, 403, Nucl. En. Agency.

Lewis, E. E., Miller, W. F., 1984. Computational methods of neutron transport. American Nuclear Society. IL. USA.

Los Alamos Scientific Laboratory Group X-6, 1979. MCNP-A general Monte-Carlo code for neutron-photon transport. Report LA-7369, Los Alamos Scientific Laboratory.

Marleau, G., Hébert, A., Roy, R., 2008. A user guide for DRAGON 3.06, Report IGE-174, 7, Institut de Génie Nucléaire, École Politechnique de Montréal, Montréal, Québec.

Piessens, R., de Doncker-Kapenga, E., Überhuber, C. W., Kahaner, D., 1983. QUADPACK: A subroutine package for automatic integration. Springer-Verlag. ISBN 978-3-540-12553-2.

Riyait, N. S., Ackroyd, R. T., 1987. The finite-element method for multigroup neutron transport: Anisotropic scattering in 1-D slab geometry. Ann. Nucl. Energy, 14(3):113-133.

Rhoades, W. A., Childs, R. L., 1993. DORT/TORT two- and three-dimensional discrete ordinates transport, Version 2.7.3. ORNL, Oak Ridge, RSIC-CCC-543.

Roy, R., 1991. Anisotropic scattering for integral transport codes. Part 2. Cyclic tracking and its application to XY lattices. Ann. Nucl. Energy, 18(9):511-524.

Saad, Y., 1994. SPARSKIT: a basic tool kit for sparse matrix computations-Version 2.

Sánchez, R., McCormick, N. J., 1982. A review of neutron transport approximations. Nucl. Sci. and Eng., 80:481-535.

Sjoden, G. E., Haghighat, A., 1996. PENTRAN, A 3-D scalable transport code with complete phase space decomposition. Trans. Am. Nucl. Soc., 74.

Spanier, J., Gelbard, E. M., 2008. Monte Carlo principles and neutron transport problems. Dover Publications. Mineloa, NY.

Stacey, W. M., 2001. Nuclear Reactor Physics. Wiley, New York.

Verdú, G., Ginestar, D., Vidal, V., Muñoz-Cobo, J. L., 1994. λ modes of the neutron diffusion equation. Ann. Nucl. Energ., 21(7):405-421.

Weinberg, A. M., Wigner, E. P., 1958. The Physical Theory of Neutron Chain Reactors. Chicago University Press, Chicago.

Wolfram Research, Inc., 2010. Mathematica, Version 8.0. Champaign, Illinois.